AIMS Energy, 9(5): 1067–1096.
DOI: 10.3934/energy.2021049
Received: 13 May 2021
Accepted: 29 September 2021
Published: 25 October 2021

http://www.aimspress.com/journal/energy

Research article

Determination of biomass combustion rate in a domestic fixed bed boiler

Mariana Vale da Silva[1], Victor Ferreira[1] and Carlos Pinho[2,*]

[1] INEGI—Instituto de Ciência e Inovação em Engenharia Mecânica e Engenharia Industrial, Porto, Portugal
[2] CEFT—DEMEC—Faculdade de Engenharia da Universidade do Porto, Porto, Portugal

* **Correspondence:** Email: ctp@fe.up.pt; Tel: +351225081747; Fax: +351225081440.

Abstract: This manuscript presents an experimental study on the combustion rate of biomass briquettes or logs in a domestic boiler, by monitoring the time decay of its mass and the temperature of the flame inside the boiler. Assuming close to steady state conditions, two combustion models were studied: the constant particle density-burning model and the constant particle diameter-burning model. For each model, the evolution of the global combustion resistance with the decay of the particle diameter was analyzed, and it was possible to conclude that the burning occurred approximately with constant particle size and that the heterogeneous C to CO reaction takes place at the surface of the inner carbonaceous core. The high values obtained for the Sherwood number revealed that there were significant convective effects inside the furnace and compare well with a previously developed Sherwood number correlation for a packed bed of active particles.

Keywords: biomass; briquettes; combustion rate; fixed bed; wood logs

1. Introduction

Portugal is a European country with high annual solar exposition leading to a high vegetable biomass production, suitable for energetic purposes [1]. The biomass to useful thermal or mechanical energy conversion can be carried out through several biochemical of thermochemical paths [2–4]. The combustion is the most used conversion process either in underdeveloped or in developed countries, mainly for cooking and domestic heating [4,5]. The use of agricultural or forestry residues as fuels for small-scale domestic heating is rather frequent either in Europe [6,7], or for more simple applications like those used in Africa [8].

The packed bed combustion of relatively large particles is dominated by the diffusion mechanism

and in the case of moving grates; the particle mixing is relevant for the combustion rate [9]. A smaller fuel particle size might guarantee a constant and steadier burning pattern, while burning larger size particles demands a more careful control of furnace operation [10]. The same research team refers in a more recent publication that this burning technique is very complicated and to get good information on bed temperature profiles and combustion gases composition, as well as to get a proper understanding about the events occurring in such type of reactor, deep computational modelling analysis is fundamental [11]. Recent studies on fixed combustion are concerned with the understanding of the impact of fuel size on the performance of wood chip-fired boilers [12,13].

There are relevant numerical studies in packed bed biomass combustion covering a wide range of conditions, since the bed compaction phenomenon [14], ignition front propagation [15] and recycled flue gas ratios [16]. Goméz et al. [17] developed a mathematical model for the simulation of large biomass particles based on their own experimental studies. Large moving or reciprocating grates were also subject of numerical studies [18,19]. However, it must be stressed that in the conclusions these lastly referred studies [14–19], the authors always refer the importance of the need to validate the numerical results with some sort of experimental data.

As far as the combustion in domestic stoves or boilers of briquettes is concerned, the studies mainly concentrate on the overall combustion behavior, emissions and stove or boiler efficiency, [20,21]. The investigation of physical and combustion properties of briquettes from cashew nut shell and cassava starch binder [22] has also been subject of interest. The importance of torrefaction to improve the quality of low-grade biomass briquettes, for subsequent use on woodstoves was analyzed by Trubetskaya et al. [23]. Experimental studies on the determination of the burning rates of waste biomass briquettes are still scarce, although the determination of the burning rate of water hyacinth briquettes with an aquatic weed binder is worth to be mentioned [24], while Hassan et al. [25] present results on the burning rate of two wood chars. Also Oyelaran et al. [26], present some information on the combustion rate of briquettes of coal and banana waste with starch binder, while Onukak et al. [27], in a study on the characterization of briquettes made from tannery wastes, also show results on the burning rate of briquettes.

Bruch et al. [28] refer the need to perform experiments on the rate of combustion of single particles, to validate more complex models on the packed-bed combustion of a finite number of wood particles. However, with few exceptions [17,29,30], experiments on small-scale fixed-bed biomass boilers are scarce and the present work is a contribution to fulfill that objective.

Even though recommendations about the reduction of the particle size to achieve a steadier combustion performance in fixed bed are frequent [10,31], many situations are dependent upon the feed-in biomass dimensions, as is the case of the combustion of briquettes and logs. The present experimental study, concerns precisely the determination of the combustion rate of solid fuel particles, obtained either from briquettes or from logs, placed on the top of a fixed bed in a domestic wood burning hot water boiler, and connects such burning rate to the combustion control mechanisms. Four different biomasses, from the Galicia-Northern Portugal Euroregion, were tested, namely, commercial briquettes, laboratory produced briquettes from pine sawdust and vine pruning wastes and eucalyptus wood logs.

2. Materials and methods

2.1. Experimental setup

The experiments were carried out in a domestic wood burning hot water boiler and the experimental set-up is in the scheme of Figure 1. There is a small Kern balance, balance 1, to weight the batches of briquettes, and a second larger balance, balance 2, from Gram, placed below the boiler. Balance 1 was also used to measure the time mass variation of a briquette during the combustion process, as detailed ahead. With balance 2 it was possible to follow the time evolution of the overall boiler mass, during any experiment.

For each experiment several temperature values were monitored, namely, the inlet and outlet water temperature, the combustion exhaust gas temperature and also the temperature in several points of the external surface of the boiler, by means of K type thermocouples. These temperatures are T1 the water inlet temperature, T2 the water outlet temperature, T3 the exhaust combustion gases temperature, T4 the flame temperature, T5 the right hand side boiler wall temperature, T6 the wall temperature at the upper boiler door, T7 the wall temperature at the lower boiler door and T8 the wall temperature at left hand side wall of the boiler, Figure 1. The flame temperature T4 was determined by inserting the corresponding thermocouple inside the lower part of the combustion chamber, the flame region, as indicated in this same figure.

For the analysis of the composition of the combustion gases three different analyzers were used: a paramagnetic oxygen analyzer from Signal; an infrared carbon dioxide analyzer from Signal, and an infrared carbon monoxide analyzer from ADC. All these combustion gas results, excepting those for oxygen, were corrected for an oxygen volumetric dry basis percentage of 13% according to the EN 14785:2008 [32], applicable to domestic heating appliances burning biomass. Two sampling probes and corresponding pumps were used. One dedicated to the oxygen analyzer and the second for the other analyzers. This increased the sampling mass flow rate sent to the oxygen analyzer improving its response time. The analyzers operated with dry combustion gases and consequently the sampled mass flows were sent previously to condensers in order to eliminate the combustion formed water in the exhaust gases. In the same scheme of Figure 1 it is also shown a water flow meter and a standard Pitot tube for the exhaust gas mass flow measurement, and the set of combustion gas analyzers.

The wood burning Solzaima boiler, model SMZ IW, has a 24 kW nominal thermal output. It is used for water heating in domestic hot water heating systems, as well as space heating through convection and radiation from its walls. Figure 2 shows a scheme of the boiler with its main external dimensions. The empty boiler weights 383 kg, has a water capacity of 73 L, and a maximum loading capacity of 30 kg of solid fuel, for a maximum briquette length of 475 mm. This figure also shows, through the boiler section view, the inverted flame operating mode of the boiler.

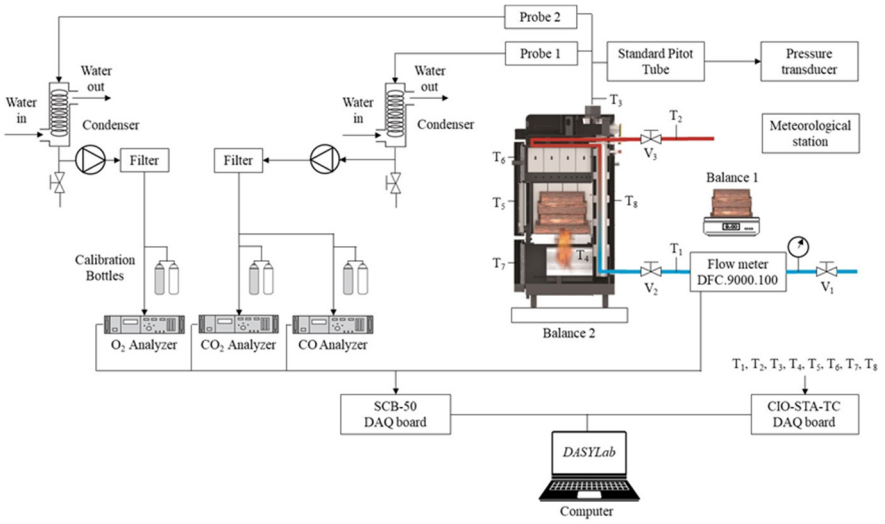

Figure 1. Schematics of the experimental set-up.

Using the DASYLab software, experimental data were collected and registered in a computer by means of a data acquisition system from Measurement Computing. Two external boards were used, the CIO-STA-TC board receiving the thermocouple data and the SCB-50 board receiving signals from the gas analyzers and the water flow meter. The data acquisition rate was of 1 Hz.

The boiler had two operating modes. The startup mode and the normal operating mode. During startup and bed ignition process, the furnace air inlet is by the blue arrows in Figure 3a). The wood logs or briquettes are placed in the combustion chamber and the air is supplied such that the combustion of C to CO and of the volatiles released from the solid burning bed takes place around it until the temperature in the upper part of the furnace is high enough to maintain a stable condition. Afterwards, the air supply flow, indicated again by the blue arrows, is like that shown in Figure 3b), and the volatiles combustion takes place downwards, while the C to CO heterogeneous phase reaction still takes place in the upper part of the furnace. In any operating situation the boiler works in forced draught mode, the combustion gases fan is in the boiler exhaust gases outlet, Figure 2.

The uncertainty values presented in Table 1 are for the molar concentrations of the gaseous components of the exhaust gas flow, whereas in Table 2 there are the uncertainties for temperature measurements, being $\boldsymbol{U_T/T}$ the corresponding relative global uncertainty. As far as the water flow rate is concerned, the random uncertainty for a confidence interval of 95% is of ±0.297 kg/min. These uncertainty values were determined according to the methodology proposed by Coleman and Steele [33].

Table 1. Global uncertainties for the molar concentration of the exhausts gas flow components.

O_2 [%]	CO_2 [%]	CO [%]	NO [%]	NO_2 [%]
±0.100	±0.200	±0.00165	±0.001	±0.001

A [mm]	B [mm]	C [mm]	D [mm]	E [mm]	F [mm]
505	1520	860	1070	50	55

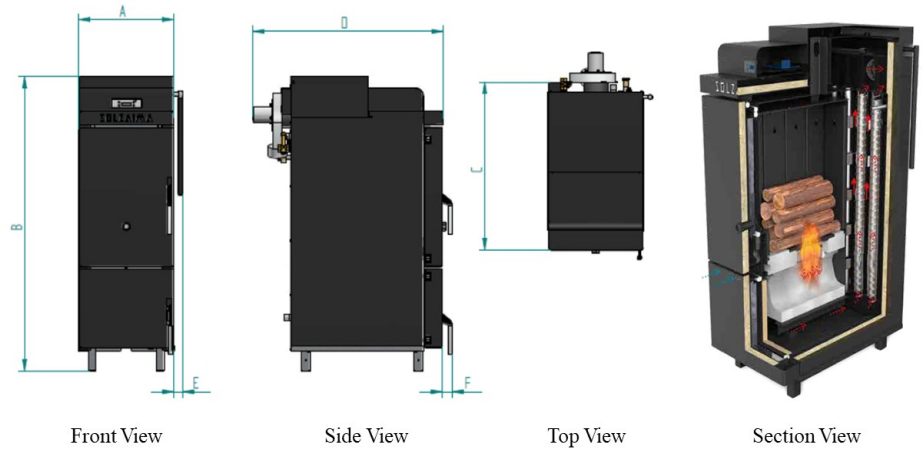

Figure 2. External dimensions of the Solzaima boiler.

Table 2. Global uncertainties for the temperature measurements.

***T* [°C]**	**14**	**38**	**85**	**110**	**630**	**950**
U_T/*T* [%]	2.44	1.37	1.16	1.14	1.10	1.10

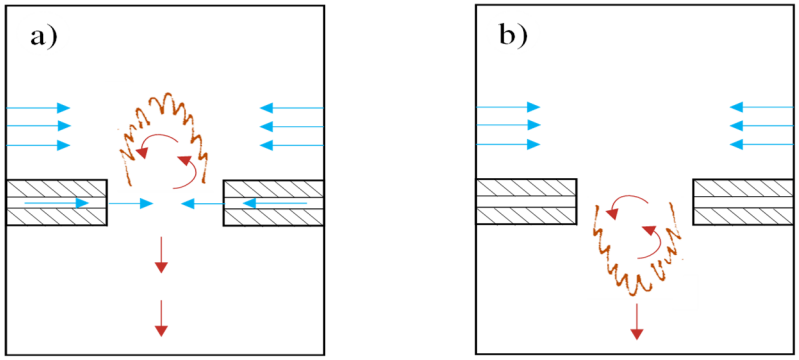

Figure 3. Schematics of operation process in the boiler furnace; a) Ignition period; b) Normal burning regime. The blue arrows represent the inlet airflow and the brown ones the combustion gas flow.

2.2. Composition of fuels

The three types of briquettes had similar and almost constant diameters and lengths, whereas the eucalyptus logs had to be cut to get the correct size. The commercial briquettes were rather heterogeneous, while those manufactured at IPV from pine sawdust and vine pruning waste were quite homogeneous.

The biomass moisture content was obtained through samples from each biofuel and its mass loss was evaluated according to the FprEN 14774-2:2009 [34]. Previously weighted samples were fully dried inside a Binder laboratory oven at 105 °C. The fuels proximate and immediate analysis as well

as the corresponding lower heating values are in Table 3.

Table 3. Characteristics of the tested fuels.

	Commercial	Pine saw-dust	Vine pruning	Eucalyptus
Moisture [% wb]	10.6	6.9	10.3	13.4
Volatile 900 °C [%]	72.8	85.4	69.5	70.7
Ash 550 °C [%]	1.2	0.7	3.2	1.0
Fixed carbon [%]	15.4	7.0	17.0	14.9
C [% db]	55.6	54.9	47.0	53.0
N_2 [% db]	3.3	0.2	0.6	0.2
H_2 [% db]	6.4	5.2	6.2	7.2
S [% db]	0.09	0.2	0.05	0.3
O_2 [% db]	34.6	39.5	46.1	39.2
HHV [MJ/kg]	19.2	19.6	20.0	18.7
LHV [MJ/kg]	17.8	18.5	18.6	17.1

For the commercial and vine pruning waste briquettes, the proximate and ultimate analysis were determined by the "Centro para a Valorização de Resíduos" (www.cvresiduos.pt). For the pine sawdust briquettes, the proximate analysis was also determined by the "Centro para a Valorização de Resíduos", whereas the ultimate analysis was from the literature [35]. For the eucalyptus wood, the moisture content was determined in the laboratory oven according to FprEN 14774-2:2009 [34] and the proximate and ultimate analysis from the literature [35,36]. The tested samples were obtained from the fuels as received and subsequently tested.

2.3. Burning rate experiments

In these burning rates experiments, a sample under analysis was taken away from the furnace to be weighted every two minutes. This sample of biomass, a part of a briquette, was placed inside a metallic mesh bag to be easily removed, weighted and subsequently placed again on the top of the burning bed. The burning bed was a batch of the briquettes of the same biomass type as the one under analysis inside the metallic mesh bag. Figure 4 shows the sample being weighted.

During weighing, the metallic bag containing the biomass sample, was placed in a bowl inside which there was a constant mass of sand. The sand is a protective shield to avoid any balance damage. In the study of the combustion rate, some simplifying assumptions were considered. To begin with, the boiler-operating regime was considered in steady state operation. It is assumed during the experiment, that the sample combustion only takes place when the sample is inside the furnace, and its combustion is quenched when the sample is outside the furnace, while the bed of the remaining briquettes undergoes its combustion process. The models adopted in the study only consider the combustion of solid carbon particles. The woody particles after being introduced in the furnace undergo an initial heating phase with moisture release, followed by pyrolysis with volatiles release and subsequent char formation. In the present study, the initial heating period until char formation took place was discarded, and only when the sample particle burned mass fraction was above 20%, the results were taken into account for the evaluation of the char combustion rate. This 20% lower limit was experimentally determined by visual observation of the sample during its external weighting

process. Its charred appearance was the evaluation criteria, as well as its mass reduction due to the combustion process. Another simplification was to consider that the particle was spherical and for such reason the sample under evaluation was cut from a briquette or a log, in order to guarantee its closeness to the spherical shape.

Figure 4. Sample weighing during a burning rate experiment.

To facilitate the combustion data analysis, it was assumed that each experiment was composed by several time intervals j, since the test beginning ($j = 0$) until its end ($j = n$), being n the total number of time intervals. At the beginning of each experiment ($j = 0$), and before placing the sample on the top of the burning bed, inside the furnace, its initial mass was measured and registered m_0. Then along the combustion process, and for each time interval j, the feeding instant $t_{in,j}$, the sample extraction instant $t_{out,j}$ and the sample mass after being extracted from the boiler furnace m_j were all measured and registered. The time counting process began at the time instant $j = 1$, by making $t_{in,1} = 0$ minutes, in all experiments that were carried out. As the burning time inside the boiler furnace was previously defined as two minutes, then Eq (1) gives the relation between the sample entrance and extraction times, in minutes,

$$t_{out,j} = t_{in,j} + 2 \qquad j = 1 \text{ to } n \tag{1}$$

The exit instant from the j interval is not equal to the entrance of the next $j + 1$ interval, the time difference that exists is the time required for the sample weighing process and to take a picture it. So, for data treatment and considering that the combustion is quenching while the sample is outside of the furnace, the time difference between $t_{out,j}$ and $t_{in,j+1}$ corresponds to a time interval that is being subtracted from the running time in order to get the real sample burning time. For each interval j it was created a fictitious time instant, corresponding to the sample mass m_j, as the time interval of the weighing process was not accounted for. The time counting started at $j = 0$, doing $t_0 = 0$ minutes. For the following time instants, the fictitious time, in minutes, was given by,

$$t_j = t_{j-1} + 2 \qquad j = 1 \text{ to } n \tag{2}$$

Following the same line of though, the total experiment duration was determined by taking into account all the time steps during which the particle is burning inside the boiler furnace, and called the effective experiment duration, is given by,

$$t_{ef} = 2n \tag{3}$$

Through the time evolution of the mass of the burning particle, it is possible to determine its burned mass fraction φ_j for each interval j, through Eq (4). At the initial time instant (j = 0), the burned mass fraction φ_0 is zero, the particle has not yet suffered any drying, pyrolysis or combustion process.

$$\varphi_j = \frac{m_0 - m_j}{m_0} \qquad j = 0 \text{ to } n \tag{4}$$

Using the mass of the sample particle under study, it is approximately true that,

$$\dot{m}_{c,j} = \frac{m_{j-1} - m_j}{t_j - t_{j-1}} \qquad j = 1 \text{ to } n \tag{5}$$

where $\dot{m}_{c,j}$ is the particle carbon burning rate in the time interval j, m_j is the sample mass at the interval j, $m_{j\text{-}1}$ is the sample mass in the previous interval $j - 1$, t_j is the fictitious time for the interval j and $t_{j\text{-}1}$ is the fictitious time for the previous interval $j - 1$. As referred, the time used in Eq (5) is the fictitious time, because, as explained, the combustion only occurs while the particle is inside the boiler furnace, and the combustion is quenched when the sample particle is outside the furnace being weighed. For any interval j, Δt is equal to two minutes, the predefined residence time of the sample particle inside the furnace.

For the analysis of this experiment, it is assumed that while burning the particle follows one of two simple mathematical models, combustion at constant particle density, or combustion at constant particle diameter. Both mathematical models consider that diffusive and convective effects are important in terms of mass transfer phenomena.

2.4. Combustion at constant particle density

In this mathematical model, it is assumed that the carbon particle burns at constant density and the ashes released during the combustion fall down from the particle and are dragged away from it. In this way the particle diameter reduces along the combustion process. The combustion reaction is thus affected by a sequence of two steps occurring in series, the oxygen mass transfer towards the particle surface and the subsequent heterogeneous phase reaction taking place at the particle surface of this oxygen with the carbon to form carbon monoxide. The slower of these two steps controls the reaction rate, thus there is a competition between the mass transfer and the heterogeneous reaction kinetics. Usually for small size particles (<100 μm) or a relatively lower particle temperature (<800 °C), the combustion is chemically controlled, whereas for higher particle temperatures (>800 °C) and larger particles, above 5 mm diameter, as it is the present case under study, the mass transfer controls the combustion reaction [37–39]. Turns [40] refers that the combustion is chemically controlled for small

particles burning at low temperatures but does not present reference values either for the particle size or the combustion temperature.

As already referred, the heterogeneous phase reaction leads to the formation of carbon monoxide, as per Eq (6),

$$\mathrm{C} + \frac{1}{2}\mathrm{O_2} \rightarrow \mathrm{CO} \tag{6}$$

while the subsequent oxidation of CO to CO_2 can happen immediately afterwards, or away from the particle surface, depending upon the particle size.

$$\mathrm{CO} + \frac{1}{2}\mathrm{O_2} \rightarrow \mathrm{CO_2} \tag{7}$$

In the first situation, the combustion is complete at the particle surface, while in the second situation the combustion is incomplete at the particle surface. When the combustion is complete it can be said that at the particle surface it occurs that,

$$\mathrm{C} + \mathrm{O_2} \rightarrow \mathrm{CO_2} \tag{8}$$

Although complete combustion at the particle surface takes place for particles above 1 mm diameter, as is the case of the briquettes under analysis, the boiler where the study was carried out was designed so that the combustion of the solid bed took place with sub stoichiometric air, thus promoting the incomplete combustion at the particles surface and leading to the CO combustion away from the bed of particles, as explained in the *modus operandi* of the boiler.

The mass rate of the combustion of a single particle $\dot{m}_c$ is given by,

$$\dot{m}_c = 12\ \pi\ d^{\,2} K\ C_\infty \tag{9}$$

where d is the carbon or char particle diameter, $1/K$ is the overall resistance to combustion and C_∞ is the molar concentration of oxygen away from the char particle, and determined by assuming a perfect gas behavior for the oxygen,

$$C_\infty = \frac{p_{O_2}}{\bar{R}\ \bar{T}_f} \tag{10}$$

p_{O_2} is the oxygen partial pressure, $\bar{R}$ is the universal gas constant and $\bar{T}_f$ is the average flame temperature close to the particle surface as read by the thermocouple and ignoring values read during the periods when the particle was outside the furnace.

Considering the steady state continuity equation for a single generic chemical species with molar concentration C_A, for spherical geometry, and radius r,

$$\frac{d}{dr}\left(r^2 \frac{dC_A}{dr}\right) = 0 \tag{11}$$

and integrating it with the following boundary conditions, $\begin{matrix} r = d/2, C_{O2} = C_s \neq 0 \\ r \to \infty, C_{O2} \to C_\infty \end{matrix}$, the oxygen concentration profile around a spherical burning particle with diameter d is given by,

$$C_{O2} = C_\infty - [C_\infty - C_s]\frac{d}{2r} \tag{12}$$

The number of kmols of O_2 going, per unit time, towards the particle surface under the diffusion mechanism is at the particle surface given by,

$$\dot{n}_{O_2} = -\pi d^2 D_g \left.\frac{dC_{O2}}{dr}\right|_{r=d/2} \tag{13}$$

where D_g is the diffusivity of oxygen in the air. Integrating it leads to,

$$\dot{n}_{O_2} = 2\pi d\ D_g\left(C_s - C_\infty\right) \tag{14}$$

or in absolute terms,

$$\left|\dot{n}_{O_2}\right| = 2\pi d\ D_g\left(C_\infty - C_s\right) \tag{15}$$

When the combustion is complete at the particle surface for each kmol of O_2 arriving at it, 1 kmol of carbon is consumed. Assuming that the heterogeneous C to CO reaction is a first order one,

$$\dot{n}_c = \pi d^2 k_c C_s \tag{16}$$

and then due to the fact that $\dot{n}_c = \left|\dot{n}_{O2}\right|$, the result is that the reaction rate can be written as,

$$\dot{n}_c = \pi d^2 K\ C_\infty \tag{17}$$

being the overall combustion resistance, $1/K$, given by,

$$\frac{1}{K} = \frac{d}{2D_g} + \frac{1}{k_c} \tag{18}$$

In the case of incomplete combustion at the particle surface, now for each ½ kmol of O_2 reaching the particle surface, 1 kmol of C is consumed,

$$\dot{n}_c = 2\ \left|\dot{n}_{O_2}\right| \tag{19}$$

and then,

$$\dot{n}_c = \pi d^2 K\ C_\infty \tag{20}$$

leads to,

$$\frac{1}{K} = \frac{d}{4\ D_g} + \frac{1}{k_c} \tag{21}$$

In general terms the carbon consumption rate is given by,

$$\dot{n}_c = \pi d^2 K\ C_\infty \tag{22}$$

being,

$$\frac{1}{K} = \frac{d}{2\ f\ D_g} + \frac{1}{k_c} \tag{23}$$

The above deduction was for pure diffusion, when *Sh* = 2. However, in broader terms the overall combustion resistance is given by,

$$\frac{1}{K} = \frac{d}{Sh\ f\ D_g} + \frac{1}{k_c} \tag{24}$$

being *Sh* the particle Sherwood number, $f = 1$ when the combustion is complete at the particle surface and $f = 2$ for the carbon to CO combustion at the particle surface, D_g is the diffusivity of oxygen in the air and k_c is the reaction rate constant for the heterogeneous phase reaction taking place at the external surface of the solid particle, C + 1/2 $O_2 \rightarrow$ CO. The two terms of the second member of Eq (24) refer to the mass transfer resistance and to the kinetics resistance and from the plot of 1/*K* versus the particle size d, information can be obtained about the combustion control. The slope gives data about the mass transfer resistance while the intercept gives information about the heterogeneous phase reaction kinetics.

After the determination of the burned mass fraction φ_j, for every interval *j*, if the combustion is assumed as taking place at constant density ρ, the sample particle diameter corresponding to this burned mass fraction is given by,

$$d_j = \left(1 - \varphi_j\right)^{1/3} d_i \tag{25}$$

where d_i is the initial diameter of the particle. The particle reaction rate for each interval *j* is then determined by means of

$$\dot{m}_{c,j} = 12\ \pi\ \left(1 - \varphi_j\right)^{2/3} d_i^{\,2} K_j C_\infty \tag{26}$$

Finally it is possible to get a set of results for all variables $\dot{m}_{Cj}$, φ_j, and d_j, for all intervals *j*, and then get K_j from Eq (26) and subsequently obtain the graphical plot of 1/K versus *d*, and according to Eq (24) to find out the slope and the intercept arriving at the relative importance of mass transfer and

reaction kinetics.

2.5. Combustion with constant particle diameter

For this mathematical model, it is assumed that the ashes formed during the combustion process do not dissolve remaining around the central core made of carbon and ashes. Thus, the particles burn at constant size keeping its approximate spherical shape. Looking at Figure 5, there is the external diameter of the particle d_s, which theoretically coincides with the particle initial diameter, and there is the diameter of the carbonaceous core d_c [41,42].

The diameter of the carbonaceous core is initially equal to the particle initial diameter and consequently to d_s, and reduces along the combustion process until reaching zero. The path followed by the oxygen molecules from the particle external surface until the surface of the reacting core will increase as the combustion process goes on, Figure 5.

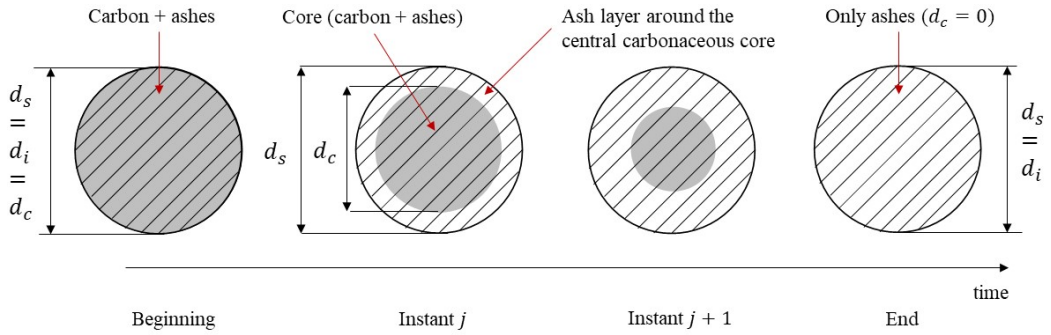

Figure 5. Time evolution of constant size combustion of a biomass particle.

According to this model the combustion process is a sequence of three steps in series, the oxygen mass transfer in the gaseous phase involving the particle till the external surface of the particle, the oxygen mass transfer through the porous ash layer around the central carbonaceous core and finally the heterogeneous phase reaction between the oxygen and the carbon and the core surface. The following subsections present this sequence of three steps.

2.5.1. Oxygen diffusion until the particle surface

Beginning with,

$$\left|\dot{n}_{O2}\right| = 4\pi r^2 D_g \frac{dC_{O2}}{dr} \tag{27}$$

and integration it for the boundary conditions $\begin{matrix} r = d/2, C_{O2} = C_s \neq 0 \\ r \to \infty, C_{O2} \to C_\infty \end{matrix}$, results in,

$$\left|\dot{n}_{O2}\right| = 2\pi D_g d_s \left(C_\infty - C_s\right) \tag{28}$$

2.5.2. Oxygen diffusion until the particle surface

Taking again Eq (27), but with D_g replaced by εD_g, where ε is the porosity of the ash layer and consequently εD_g is the oxygen diffusivity in this layer [41–44] and integration it for the boundary conditions, $\begin{matrix} r = d_s/2 \\ r = d_c/2 \end{matrix}, \begin{matrix} C_{O2} = C_s \\ C_{O2} \to C_c \end{matrix}$, results in,

$$\left|\dot{n}_{O2}\right| = 2\pi\varepsilon D_g\left(C_\infty - C_s\right)\frac{d_s d_c}{d_s - d_c} \tag{29}$$

2.5.3. Heterogeneous reaction C + 1/2 O_2 → CO at the surface of the carbonaceous core

Now taking into account the kinetics of the heterogeneous reaction, assuming again a first order reaction,

$$\dot{n}_c = \pi d_c^{\,2} k_c C_c \tag{30}$$

and paying attention that $f\left|\dot{n}_{O2}\right| = \dot{n}_c$, with f = 1 for complete C to CO_2 combustion at the carbonaceous nucleus and f = 2 for the C to CO combustion, the carbon consumption rate can be determined by

$$\dot{n}_c = \pi d_c^{\,2} K C_\infty \tag{31}$$

with,

$$\frac{1}{K} = \frac{d_c^{\,2}}{2f D_g d_s} + \frac{d_c\left(d_s - d_c\right)}{2f\varepsilon D_g d_s} + \frac{1}{k_c} \tag{32}$$

The combustion reaction rate is given by Eq (33) below. It depends on the diameter of the carbonaceous core and on the overall resistance to combustion, Eq (34), where once again the pure diffusion condition Sh = 2, was extrapolated for different values of the Sherwood number,

$$\dot{m}_c = 12\ \pi\ d_c^{\,2} K\ C_\infty \tag{33}$$

$$\frac{1}{K} = \frac{d_c^{\,2}}{Sh\ f D_g d_s} + \frac{d_c\left(d_s - d_c\right)}{Sh\ f\varepsilon D_g d_s} + \frac{1}{k_c} \tag{34}$$

The overall resistance to combustion 1/K has three terms, the first is the resistance to the oxygen mass transfer towards the particle external surface, the second concerns the resistance of the oxygen mass transfer inside the ash layer with porosity ε from the external surface of the particle until the surface of the carbonaceous core. Finally, the last term is the kinetic resistance of the heterogeneous

phase carbon oxidation to carbon monoxide. The objective of the present study is to get a plot of $1/K$ versus d_c, to get information on the relative importance of these three mechanisms.

The diameter of the carbonaceous core can be determined by means of a simple approximation. The total mass of the burning particle for the instant j is given by,

$$m_j = \frac{\pi\ d_c^{\ 3}}{6}\rho_{p,j} \tag{35}$$

where $\rho_{p,j}$ is the average density of the particle at any instant j. It is a weighted average of the density of the ash layer around the central carbonaceous core and the density of such carbonaceous core, according to the corresponding masses at the j time instant. So, the mass of the particle can be determined, also for the time instant j through,

$$m_j = \frac{\pi\ d_{c,n}^{\ 3}}{c}\rho_c + \frac{\pi\ \left(d_s^{\ 3} - d_{c,j}^{\ 3}\right)}{6}\rho_a \tag{36}$$

where ρ_c is the density of the carbonaceous core and ρ_a is the density of the ash layer around the central core. The mass of the particle is thus the summation of two terms. Assuming that the weight of the ash layer can be neglected when compared with the core mass, then it can be considered that for the instant j the mass of the particle is simply,

$$m_j = \frac{\pi\ d_{c,n}^{\ 3}}{c}\rho_c \tag{37}$$

At the beginning of the combustion, when $d_c = d_s$, from the Eqs (35) and (37) it is known that,

$$\rho_c = \rho_{p,0} \tag{38}$$

where $\rho_{p,0}$ is the particle density at the first time instant ($j = 0$). In other words, the core density is constant and equal to the initial density of the particle. Combining Eqs (35) and (37), for any instant j, an expression to determine the diameter of the carbonaceous core is obtained,

$$d_{c,j} = d_c\left(\frac{\rho_{p,j}}{\rho_{p,0}}\right)^{1/3} \tag{39}$$

which can be rewritten by taking into account the burned mass fraction φ_j for the time instant j,

$$d_{c,j} = d_s\left(1 - \varphi_j\right)^{1/3} \tag{40}$$

where d_s is the particle surface diameter. It can be concluded that Eq (40), for the calculation of the diameter of the carbonaceous core in the mathematical model for constant density combustion, is equal to Eq (25) used for the calculation of the particle diameter, in the constant density combustion model. As the diameter time evolution is identical, Eq (33) is numerically equal to Eq (26), leading to the

same numerical value for the overall resistance to the combustion for both mathematical models. What is different is the corresponding definition of the overall combustion resistance:

- For the constant density mathematical model the overall combustion resistance $1/K$ has two terms, Eq (24), being $1/K$ linearly dependent on the particle diameter;

- For the constant diameter mathematical model, the overall combustion resistance $1/K$ has three terms, Eq (34), and presents a quadratic dependence on the carbonaceous core diameter, Eq (41),

$$\frac{1}{K} = \frac{d_c^{\,2}}{Sh\, f\, D_g d_s}\left(1 - \frac{1}{\varepsilon}\right) + \frac{d_c}{Sh\, f \varepsilon D_g} + \frac{1}{k_c} \tag{41}$$

It must be stressed once more, that this mathematical analysis is very simplistic although allowing getting a quick overall idea about the resistances affecting the rate of combustion.

3. Results and discussion

To carry out the burning rate experiments the boiler was operation in steady state conditions for at least one hour. During the experiments besides the process of taking the sample out of the furnace to be weighed and its subsequent reintroduction in the furnace, the normal boiler furnace feeding procedure was also carried out, i.e., about 1 kg every 15 minutes.

The experiments were done with commercial briquettes (experiments C3 to C6), briquettes made with pine saw dust (experiment P1), with briquettes made with vine pruning wastes (experiment V1) and with eucalyptus (experiments E1 and E2).

As already explained it is assumed that the combustion reaction only takes place when the biomass sample is inside the boiler furnace and consequently the determination of the average measured parameters excludes all data during the weighing and photographing phases, in other words the time intervals $t_{out,j}$ and $t_{in,j+1}$ are not considered.

3.1. Overall results

Figure 6 shows the time evolution of the combustion exhaust gases temperature as well as the oxygen and carbon dioxide molar fractions in the exhaust gases, all for the experiment C6. The vertical dot lines are the limits of the excluded periods that concern the sample weighing process.

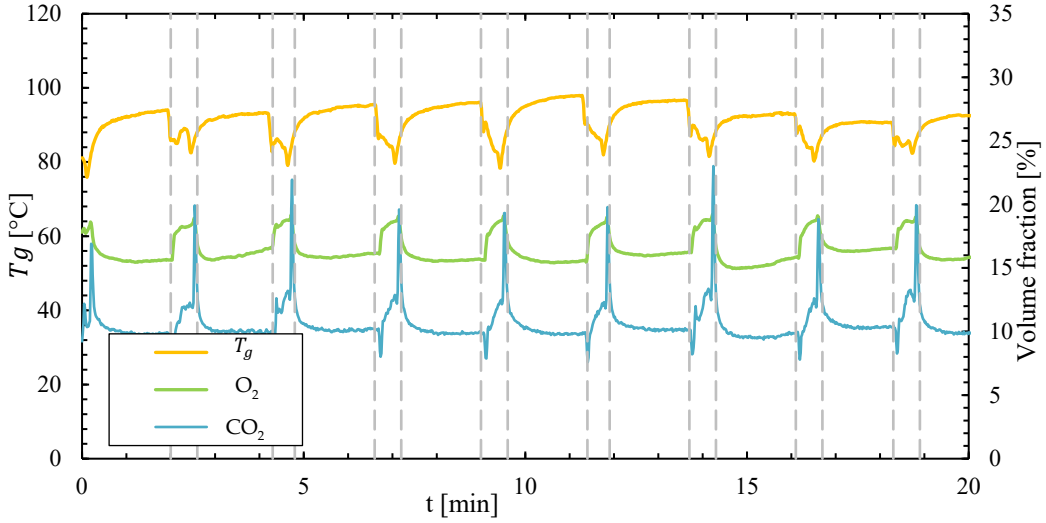

Figure 6. Time evolution of the temperature, of the oxygen and carbon dioxide volume fraction, of the exhaust combustion gases. The CO_2 is corrected for 13% (v/v) O_2. Data for test C6.

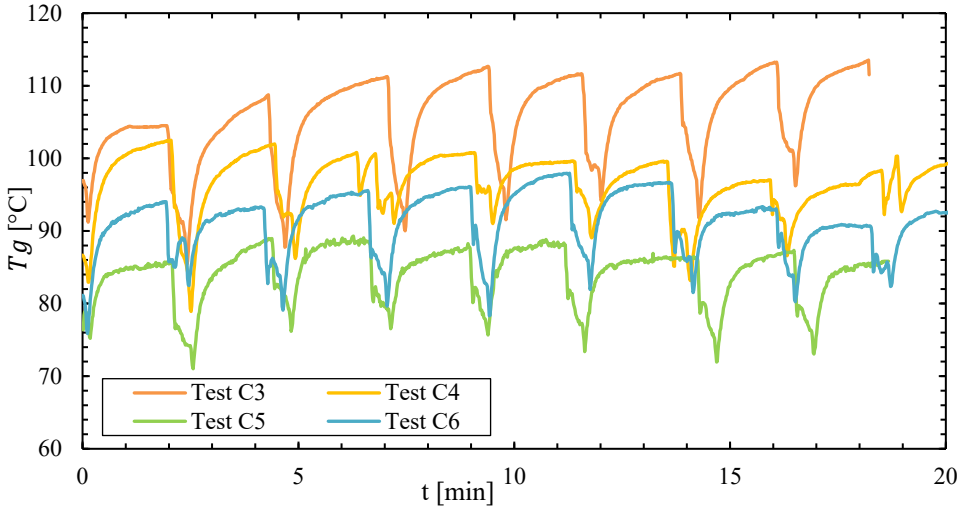

Figure 7. Time evolution of the exhaust gas temperature for tests C3, C4, C5 and C6.

Figures 7 and 8 show the time evolution of the exhaust gases temperature for the several biomasses that were tested during the combustion rate experiments, namely for tests C3, C4, C5, C6, P1, E1, E2 and V1. In Figure 9, there is the time evolution of the CO concentration in the exhaust gas flow for tests C3, C4, E1 and E2. As previously explained, there are temperature and gas concentration oscillations during the door opening periods. It was necessary to be careful and avoid any layout disturbances on the furnace fuel bed in order to guarantee an approach as good as possible to the desired steady state burning conditions. However, in global terms, it can be concluded from the observation of these figures that steady state operation conditions can be assumed.

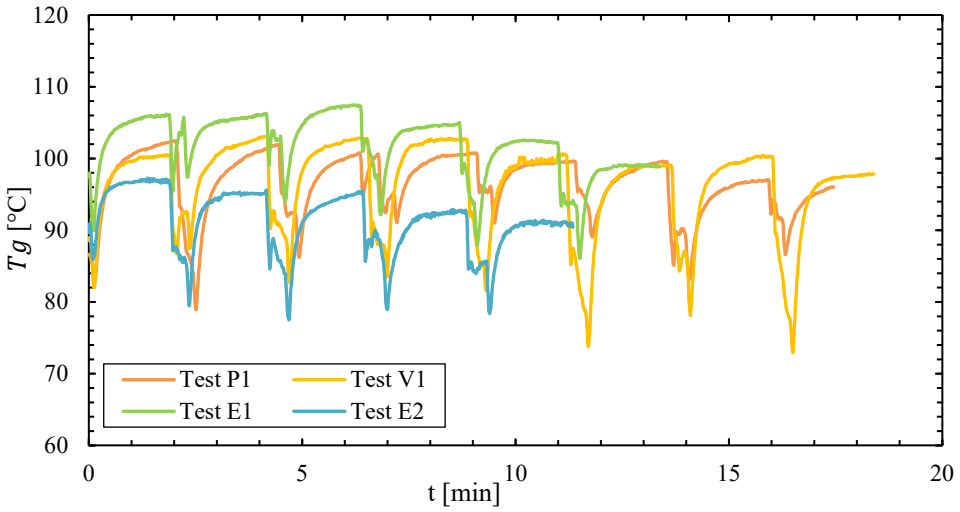

Figure 8. Time evolution of the exhaust gas temperature for tests E1, E2, P1 and V1.

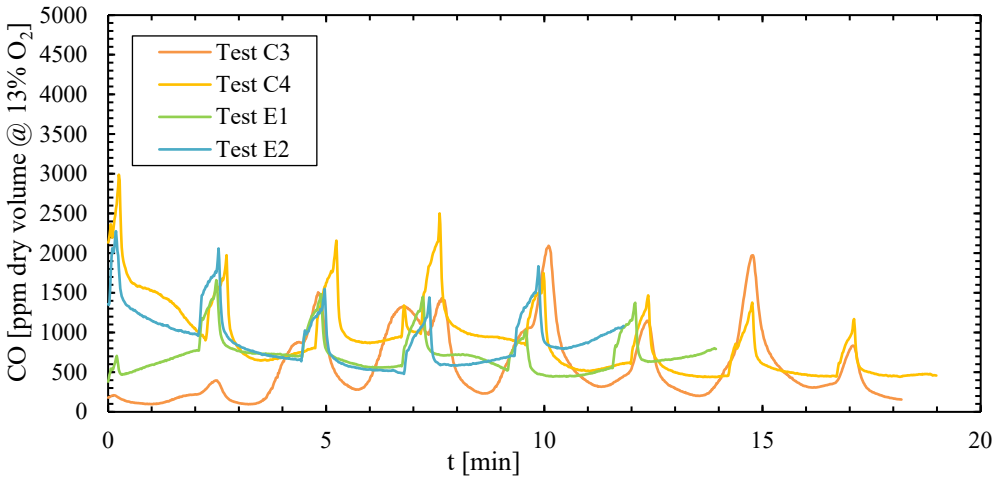

Figure 9. Time evolution of the exhaust gas CO concentration for tests C3, C4, E1 and E2.

Figure 10 presents the time evolution of the water inlet and outlet temperatures and of its mass flow rate, for test C4. Due the thermal inertia of the boiler, namely considering its large mass including the water contained in it, the time fluctuations verified in the gaseous exhaust temperature and components concentrations do not appear here. The plots in Figure 10 clearly demonstrate the steadiness of the whole process as far as the water flow and the thermal boiler output are concerned.

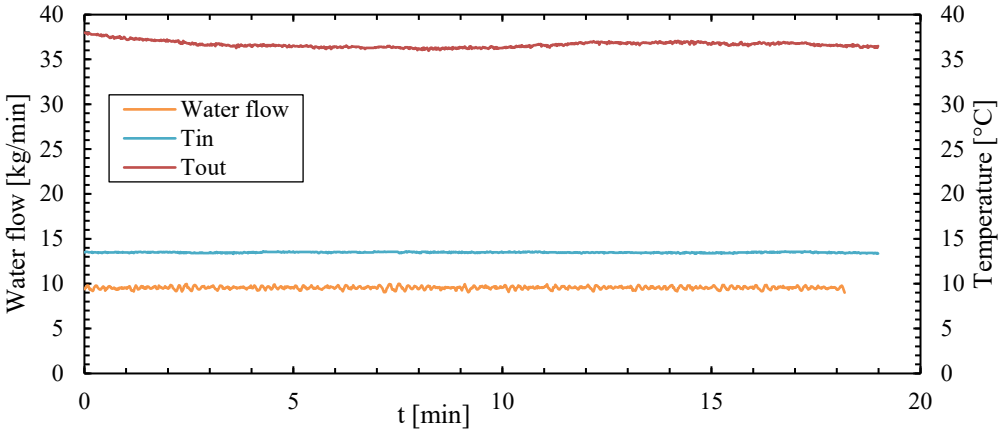

Figure 10. Time evolution of the water inlet and outlet temperature, as well as its mass flow rate for test C4.

Figures 11 and 12 present the flame temperature on the burning bed of briquettes for the tests under consideration. There are large temperature differences on the flame close to the bed of burning particles, which means that in strict terms it is almost impossible to consider that the combustion was carried out under perfect steady state operation. However in broad terms one can be said, by looking at these figures under a simplistic approach, that the burning conditions are almost steady, as temperatures, although fluctuating the evolve through a more or less constant band of values. In rough terms it can be assumed that the experiments managed to get steady state conditions.

As already explained for each time interval j the sample mass m_j was registered, the time instant of the sample extraction $t_{out,j}$, and reintroduction in the furnace $t_{in,j+1}$, and subsequently the burned mass fraction φ_j and the sample particle combustion rate $\dot{m}_{cj}$ were calculated.

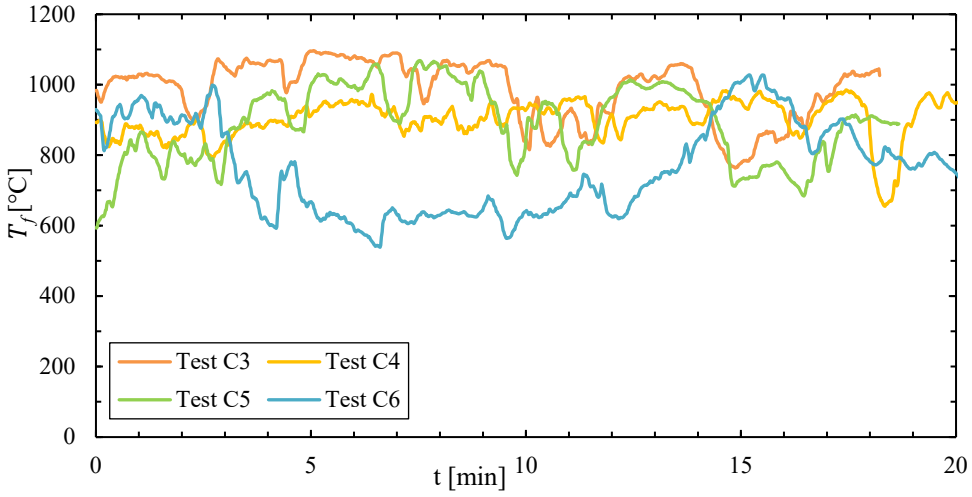

Figure 11. Time evolution of the bed flame temperature for tests C3, C4, C5 and C6.

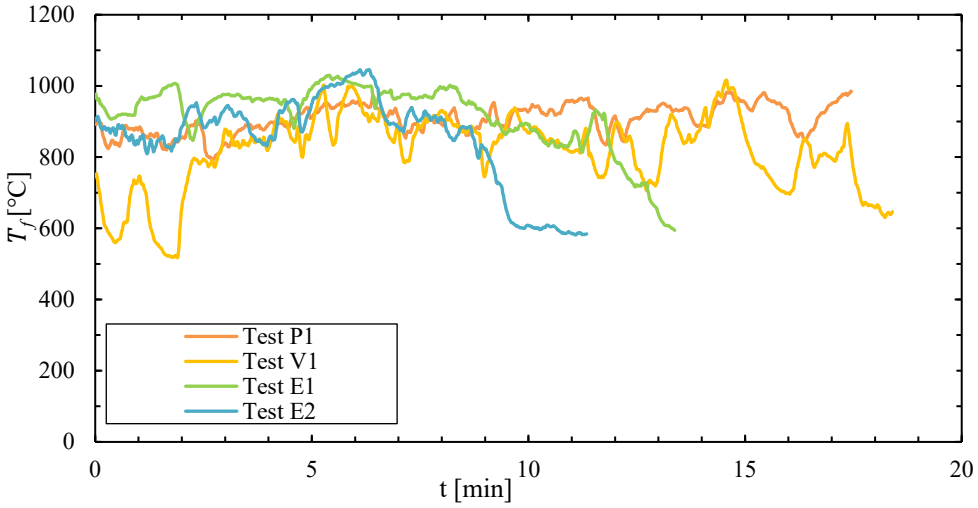

Figure 12. Time evolution of the bed flame temperature for tests E1, E2, P1 and V1.

Figure 13 shows the evolution of the burned mass fraction φ with the fictitious burning time and it is clear from the correlation coefficients of the applied trend lines, that there is a strong linear tendency. From the slope of the linear fittings presented in Figure 13 some simple conclusions can be drawn. Taking into account that a higher slope means a faster combustion, the pine (P1) and vine (V1) briquettes have all a very similar behavior, meaning that there is similar burning velocity for all these cases. On the other end, the eucalyptus logs have a higher slope. This can be explained by the fact that the eucalyptus wood is denser than the briquettes and thus, for the same particle size reduction, there is a stronger mass reduction.

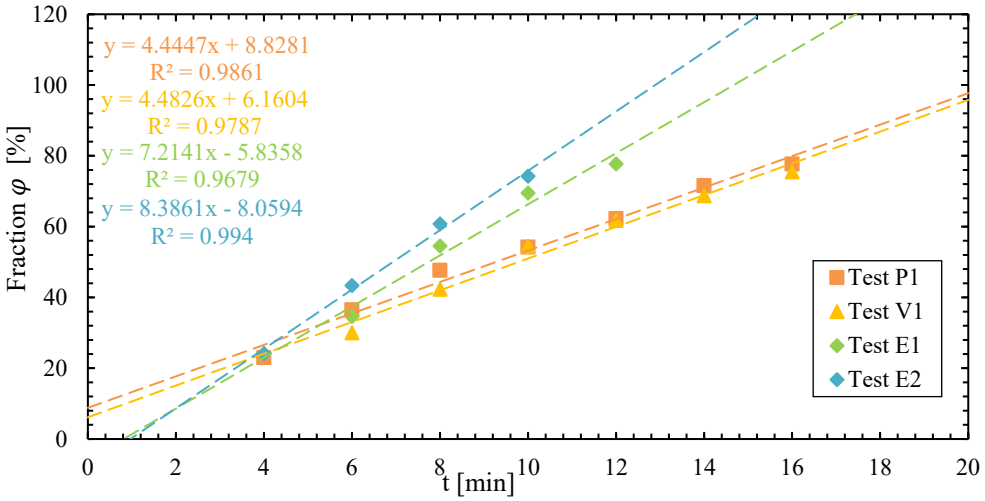

Figure 13. Time evolution of the burned mass fraction for tests E1, E2, P1 and V1.

Figure 14 gives the average slope obtained from the plots of the burned mass fraction as a function of the measured average flame temperature, and for all the briquettes experiments the slope is

approximately constant and independent of the flame temperature, whereas the eucalyptus slopes clearly distinct and decreasing with the increase on the flame temperature. For the briquettes it can be said that as expected for burning particles above 5 mm the combustion rate is not dependent upon the bed temperature, thus the expectancy is that the combustion will be mass transfer controlled. As far as the eucalyptus is concerned, it seems that there is some dependence on the bed temperature, although these two plots are insufficient to achieve a clear conclusion.

The next step is the analysis of the experimental results under the two theoretical models previously described: combustion at constant particle density and combustion at constant particle diameter. Looking at the results the conclusion was that the combustion of these briquettes took place at constant size and consequently at reducing ρ. Figure 15 shows a sequence of photographs from pine dust briquettes combustion, experiment P1, for a series of time sampling instants. Each time instant j corresponds to a fictitious burning time $t_j = 2j$, in minutes. The two initial instants, pictures with red dots, were excluded for the subsequent analysis, the corresponding burning fraction was below 20%, and the particles show no superficial carbonized appearance.

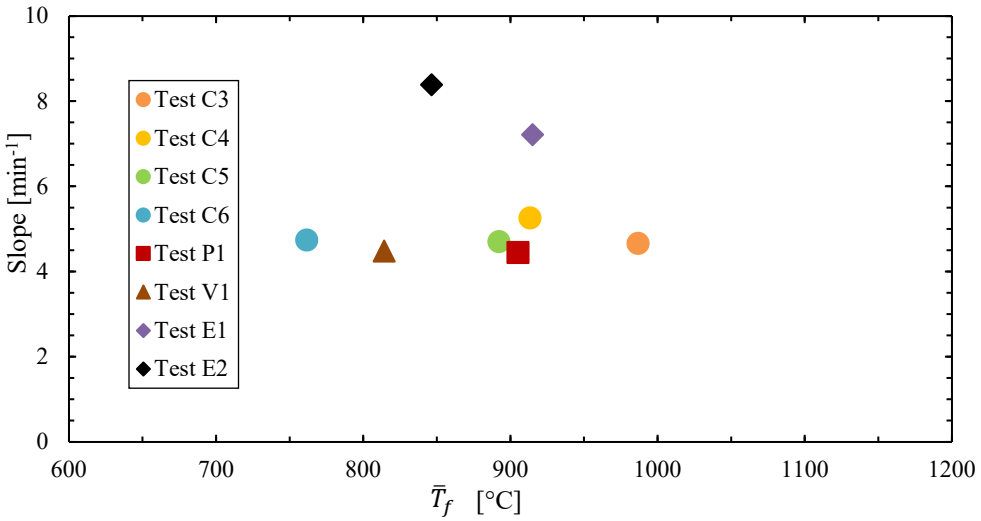

Figure 14. Average slope as a function of the average flame temperature.

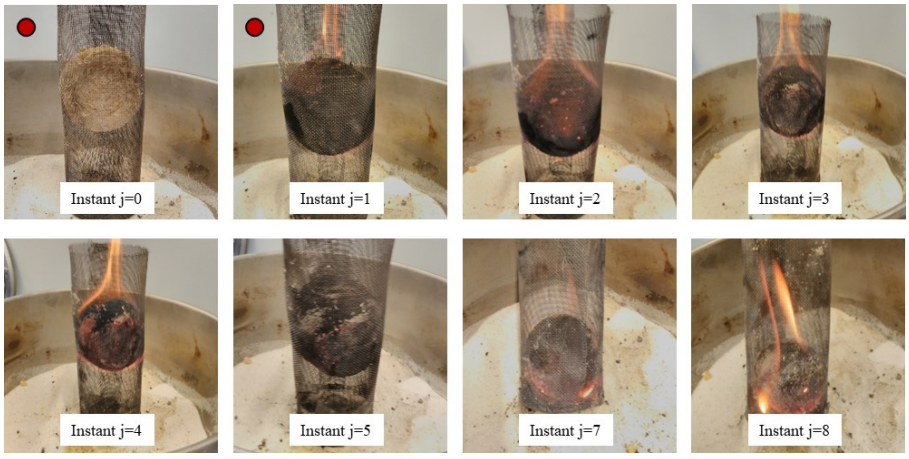

Figure 15. Pictures of the sample during test P1.

It is quite clear, looking at the sequence of pictures in Figure 15, that it can be assumed that the briquette portion under consideration burns at constant size. However, in the treatment of the experimental data the two models of combustion were taken into account, to find out which one was the most adequate.

3.2. Evaluation of combustion data under the constant density model

The experimental results of the rate of combustion were then analyzed according to the constant density model explained in section 2.4. For this analysis tables with all the parameters $\dot{m}_{Cj}$, φ_j, d_j and K_j, for the considered time intervals j were built to obtain the evolution of $1/K$ with the particle diameter d. This evolution of $1/K$ with the particle diameter d, for all intervals j, is plotted in Figure 16. For the linear fitting, abnormal observations were eliminated according to the Chauvenet criterion [45].

Table 4. Results considering a constant density combustion.

Test	$\overline{T}_f$ [°C]	C_∞ [kmol/m^3]	D_g [m^2/s]	Sh	k_c [m/s]
C3	986.8	2.03E-03	2.27E-04	−118.66	0.270
C4	913.4	2.14E-03	2.05E-04	−178.11	0.341
C5	892.2	2.15E-03	1.99E-04	−41.34	0.173
C6	761.6	2.45E-03	1.64E-04	81.49	1.535
P1	905.2	2.14E-03	2.03E-04	70.61	1.066
V1	814.2	2.30E-03	1.78E-04	−404.41	0.343
E1	846.4	2.23E-03	1.86E-04	92.143	1.856
E2	915.0	2.12E-03	2.06E-04	171.99	1.347

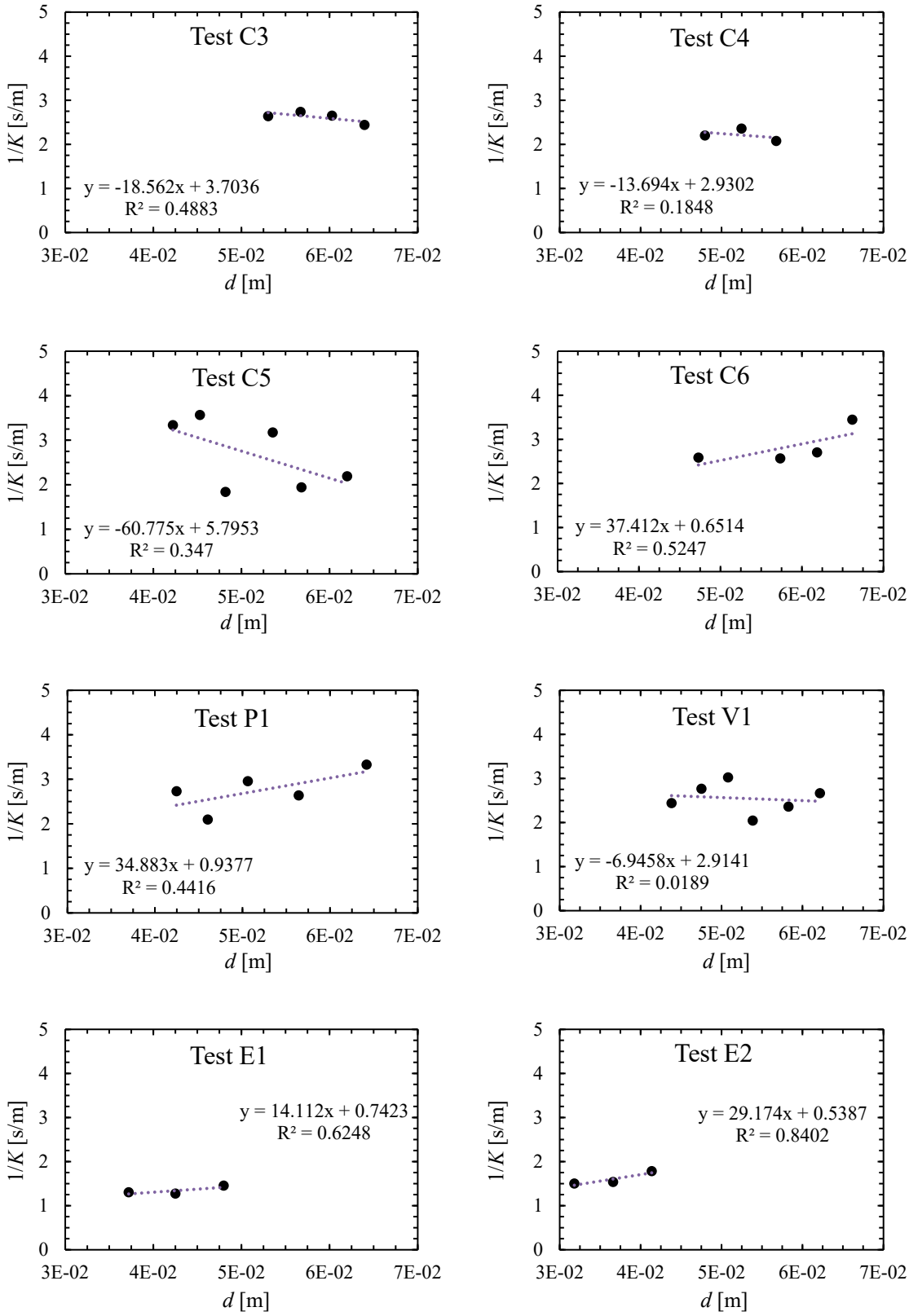

Figure 16. Evolution of the overall combustion resistance with particle diameter according to the constant density model.

Taking into account Eq (11), and the resulting linear fitting equations between the overall combustion resistance and the particle diameter shown in Figure 16, the Sherwood number *Sh* and the heterogeneous phase reaction rate constant k_c were determined. Such values are shown in Table 4 for all experiments done, as well as the corresponding average flame temperature $\bar{T}_f$, molecular concentration of oxygen far from the burning particle C_∞ and oxygen diffusivity in the gas phase D_g. The presented Sherwood numbers were calculated with the correction factor $f = 2$, considering, as previously referred, that the carbon burns to CO at the particle surface.

Table 4 shows that half the experiments led to negative Sherwood numbers (underlined values), an absurd situation in physical terms. This is easily observed in Figure 16, where the tests C3, C4, C5 and V1 have trend lines with negative slopes, while the physically correct situation must have a positive slope, as understood from Eq (24). It is clear that the combustion does not occur at constant density, which was corroborated by the pictures that were taken to the burning particles. The images of Figure 15, corresponding to the test P1, clearly show a constant particle size combustion.

3.3. Evaluation of combustion data under the constant size model

Now the same experimental results are analyzed under the constant size combustion model parameters, as presented in section 2.5. The carbonaceous nucleus diameter d_n and the overall combustion resistance values $1/K$ are the same as considered before for the constant density combustion analysis.

Figure 17 represents the overall combustion resistance $1/K$ versus the carbonaceous nucleus diameter d_c, again for all intervals *j*. Based on Eq (41), it is clear that the relation between these two parameters is a quadratic one. Accordingly, for each experiment, the quadratic fitting is applied. The corresponding correlation coefficient is also shown and again, abnormal situations were discarded according to the Chauvenet criterion [45].

For this analysis it was assumed that the combustion was controlled by the mass transfer of oxygen towards the burning particle, i.e., $1/k_c = 0$. This simplifying assumption is based on the fact that for large particles the mass transfer is the dominating mechanism of the overall combustion process [9,37–39]. It must also be stressed that for the previous analysis of the constant density combustion, this same approach was taken into account, by imposing an intercept zero, $1/k_c = 0$, but it lead to negative correlation coefficients, and this condition was then discarded. Table 5 gives the resulting Sherwood numbers for this new evaluation.

Once more, applying the Chauvenet criterion [45] to the Sherwood numbers in Table 5, the experiment C5 has a Sherwood number of 173.77 which is rather different from the other values shown in the table, that are in the 50 to 106 range of values. There is still some variability, which is understandable regarding the experimental uncertainties.

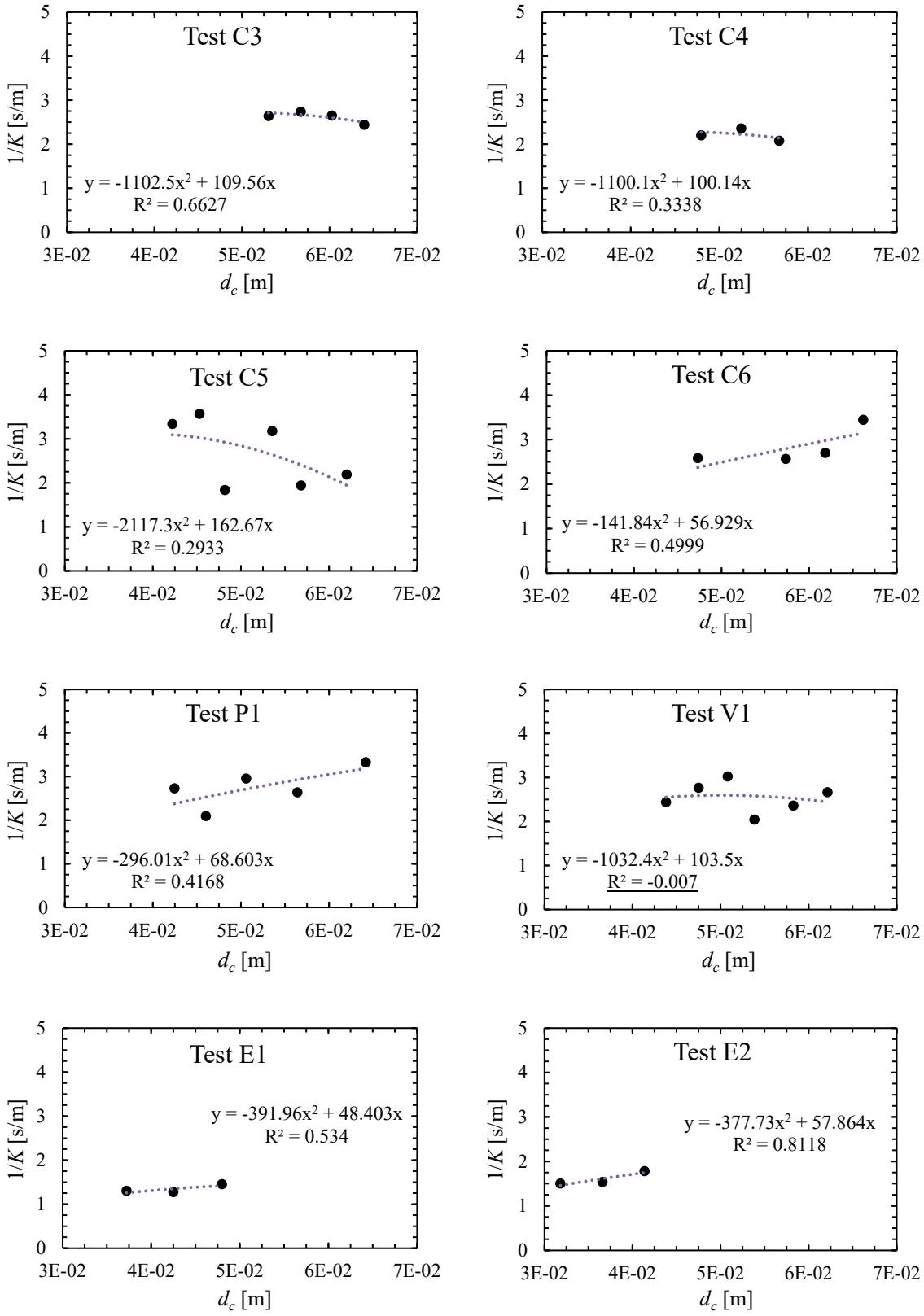

Figure 17. Evolution of the overall combustion resistance with particle diameter according to the constant size model.

Table 5. Results considering constant particle size combustion.

Test	ε	Sh
C3	0.262	76.62
C4	0.229	106.45
C5	0.089	173.77
C6	0.820	65.28
P1	0.698	51.44
E1	0.674	68.97
E2	0.552	90.81

To try to evaluate the correctness of the *Sh* values obtained in Table 5 the correlation proposed by Wakao and Funazkri [46] was used to determine the Reynolds numbers of the gas flow around the burning particle, Eq (42). These authors developed a correlation between the Sherwood and the Reynolds number for a packed bed of active particles, like the present situation concerning a bed of burning particles.

$$Sh = 2 + 1.1\, Re_d^{0.6}\, Sc^{1/3} \quad \text{for} \quad 3 < Re_d < 10{,}000 \tag{42}$$

In the above equation Re_d is the Reynolds number based on the diameter of the burning particle, and *Sc* is the Schmidt number. For a single particle under pure diffusive conditions, the Sherwood number takes the value of 2. However, in the present situation the impact of the convective phenomena inside the furnace is quite heavy, as the values in Table 5 clearly show, and also because the boiler operates in exhaust gas forced regime.

So, starting with each Sherwood number of Table 5, the corresponding Reynolds number was calculated by means of Eq (42). To do it, the Schmidt number was considered 0.73, as suggested by Bormand and Ragland [47]. Then, from the obtained Reynolds numbers, it was possible to calculate the flow velocity around the particle through Eq (43).

$$Re_d = \frac{\rho\, u\, d}{\mu} \tag{43}$$

For this last equation, air properties were assumed. Namely ρ is the air density, μ is the air dynamic viscosity and u is the flow velocity at the close average of the burning particle of external diameter d, i.e., a bed interstitial velocity. Looking at Figure 6, the average O_2 values in the exhaust gases are around 15–16% (v/v), indicating a combustion with high excess air values, justifying the approach of using air property values. The objective is to find out whether the value obtained for the gas velocity nearby the particle is a reasonable one. The air properties depend on the temperature in the close neighborhood of the particle, a value difficult to measure because of the sequence of movements of particle introduction and extraction from the bed. The only measured temperature, as already referred, was the flame temperature close to the burning bed, in the lower part of the combustion chamber, while the particle was in the upper chamber, on the top of the bed. Therefore, for the gas, mainly air, flow around the particle two temperature values were chosen, 500 and 700 °C, to find out the influence of this temperature on the obtained interstitial velocity. The air properties at these three temperature

values were obtained from the technical literature [48]. Table 6 shows the obtained values for the Reynolds numbers and subsequent air velocities nearby the burning particle.

There is some variability of the results but with the exception of the results from the C5 experiment, the values obtained for the velocity close to the burning particle, an interstitial velocity, are on the range of 0.5 to 1.6 m/s. Through the analysis of the combustion mass balance calculations, the average mass flow rate of combustion air is of 103.5 kg/h. Thus, taking into account the furnace cross section area of 0.130 m^2 (0.476 m length and 0.273 m width) and a bed porosity of 0.45, it results in interstitial velocities of 1.08 and 1.35 m/s, respectively at 500 and 700 ℃. So, the mass transfer results through the *Sh* number, and the Wakao and Funazkri correlation [46], lead to interstitial velocities of the same order of magnitude of those found through the combustion mass balance. Therefore, the present study resulted into a set of data that allow the comprehension and the definition of the mechanism controlling the fixed bed combustion of these biomass briquettes and wood logs.

Table 6. Estimated values for the bed interstitial flow velocity close to the burning sample particle.

Test	d [mm]	Re	$u_{500\ ℃}$ [m/s]	$u_{700\ ℃}$ [m/s]
C3	73.3	1344	1.5	0.9
C4	70.3	2354	2.7	1.6
C5	70.0	5393	6.2	3.7
C6	72.1	1021	1.1	0.7
P1	70.0	676.7	0.8	0.5
E1	50.0	1122	1.8	1.1
E2	55.3	1796	2.6	1.6

4. Conclusions

The determination of the combustion rate of woody particles in a domestic boiler fixed bed was carried out by assuming a steady state operation of the boiler, the combustion quenching during the particle weighing process and the spherical shape of the particle under observation. For a burning mass fraction above 20% it could be assumed, through visual inspection, that the fuel particles had undergone carbonization and consequently it was considered that, beyond that border, it was occurring the combustion of large char particles.

Through the measurement of the rate of mass consumption of sample particles, periodically withdrawn from the top of the burning fixed bed of briquettes or wood logs, it was found that the combustion experiments exhibited independence from the average bed flame temperature, showing a similar burning rate for all of them. The reduced dependence of the burning rate with temperature indicates that the kinetic control was small and transport phenomena mechanisms were dominant. The higher slopes for the combustion of eucalyptus logs are due to its higher density, leading to a stronger mass consumption for the same particle diameter reduction.

Considering the inverted flame-operating mode of the boiler, it means that carbon burned to carbon monoxide at the particle or core surface, and then CO burned to carbon dioxide away from the burning particle. The combustion occurred at constant size and reducing density, having the particles a reducing carbonaceous core and a constant size non-disaggregating ash layer involving it. The

analysis of photographs from the particles during the weighing process corroborates this conclusion.

Starting with the Sherwood values obtained from the reaction rate of the sample particle, mainly in the 50 to 106 range, and the overall resistance to combustion, and through a mass transfer correlation for this dimensionless number, applicable at packed beds of reacting particles, estimations for the gas velocities close to the sample particle were calculated and compared well to those obtained from the combustion mass balance.

The present approach and experimental methodology allowed the determination of relevant information concerning the fixed bed combustion of relatively large sized woody particles. However, future work should consider the possibility of continuously measuring the time evolution of the burning particle without extracting it from the furnace interior, by means of a dynamometer setup.

Acknowledgments

The authors are thankful to INEGI—Instituto de Ciência e Inovação em Engenharia Mecânica e Engenharia Industrial—an interface institute from the Faculty of Engineering of the University of Porto, for the administrative support and extra financial help, to carry out this work.

The present work was supported by the INTERREG Project N. PR321705—BIOMASA_AP and carried out in the Combustion Laboratory of INEGI.

Conflict of interest

The authors declare no conflict of interest. The funders had no role in the design of the study; in the collection, analyses, or interpretation of data; in the writing of the manuscript, or in the decision to publish the results.

Author contributions

MVS, VF and CP designed the experiments; MVS and VF performed the experiments; MVS carried out data curation; CP was the overall supervisor; MVS, VF and CP shared the writing, review and editing of the present text. All authors have read and agreed to the published version of the manuscript.

References

1. Ferreira S, Monteiro E, Britos P, et al. (2017) Biomass resources in Portugal: Current status and prospects. *Renewable Sustainable Energy Rev* 78: 1221–1235.
2. Van Loo S, Koppejan J (2008) *The Handbook of Biomass Combustion and Co-firing*, 2nd Ed., London, United Kingdom: Earthscan.
3. McGowan T, Bulpitt W, Brown M, et al. (2009) *Biomass and Alternate Fuel Systems—An Engineering and Economic Guide*, New Jersey, USA: Wiley.
4. Pradhan P, Mahajani S, Arora A (2018) Production and utilization of fuel pellets from biomass: A review. *Fuel Process Technol* 181: 215–232.
5. Saidur R, Abdelaziz EA, Demirbas A, et al. (2011) A review on biomass as a fuel for boilers. *Renewable Sustainable Energy Rev* 15: 2262–2289.

6. Mitchell EJS, Gudka B, Whittaker C, et al. (2020) The use of agricultural residues, wood briquettes and logs for small-scale domestic heating. *Fuel Process Technol* 210: 106552.
7. Werther J, Saenger M, Hartge E, et al. (2000) Combustion of agricultural residues. *Prog Energy Combust Sci* 26: 1–27.
8. Lubwama M, Yiga VA, Muhairwe F, et al. (2020) Physical and combustion properties of agricultural residue bio-char bio-composite briquettes as sustainable domestic energy sources. *Renewable Energy* 148: 1002–1016.
9. Yang YB, Lim CN, Goodfellow J, et al. (2005) A diffusion model for particle mixing in a packed bed of burning solids. *Fuel* 84: 213–225.
10. Yang YB, Ryu C, Khor A, et al. (2005) Fuel size effect on pinewood combustion in a packed bed. *Fuel* 84: 2026–2038.
11. Le A, Hai LX, Sharifi VN, et al. (2007) System approach from biomass combustion in packed bed reactor. *AJChE* 7: 16–29.
12. Caposciutti G, Barontini F, Francesconi M, et al. (2017) Experimental investigation on the fixed bed of a small size biomass boiler. *Energy Proc* 142: 468–473.
13. Caposciutti G, Barontini F, Galletti C, et al. (2020) Woodchip size effect on combustion temperatures and volatiles in a small-scale fixed bed biomass boiler. *Renewable Energy* 151: 161–174.
14. Gómez MA, Porteiro J, Patiño D, et al. (2014) CFD modelling of thermal conversion and packed bed compaction in biomass combustion. *Fuel* 11:716–732.
15. Karim MR, Naser J (2018) Numerical study of the ignition front propagation of different pelletised biomass in a packed bed furnace. *Appl Therm Eng* 128: 772–784.
16. Karim MR, Bhuiyan AA, Naser J (2018) Effect of recycled flue gas ratios for pellet type biomass combustion in a packed bed furnace. *Int J Heat Mass Transfer* 120: 1031–1043.
17. Gómez MA, Porteiro J, Chapela S, et al. (2018) An Eulerian model for the simulation of thermal conversion of a single large biomass particle. *Fuel* 220: 671–681.
18. Karim MR, Naser J (2018) CFD modelling of combustion and associated emission of wet woody biomass in a 4 MW moving grate boiler. *Fuel* 222: 656–674.
19. Karim MR, Bhuiyan AA, Sarhan AAR, et al. (2020) CFD simulation of biomass thermal conversion under air/oxy-fuel conditions in a reciprocating boiler. *Renewable Energy* 146: 1416–1428.
20. Roy MM, Corscadden KW (2012) An experimental study of combustion and emissions of biomass briquettes in a domestic wood stove. *Appl Energy* 99: 206–212.
21. Silva MV, Ferreira V, Sanches A, et al. (2019) Thermal Performance and Combustion Hygiene of a Briquette Burning Domestic Boiler. *Revista Mecânica Experimental (Experimental Mechanics Revue)* 31: 61–72.
22. Kimutai SK, Kimutai IK (2019) Investigation of physical and combustion properties of briquettes from cashew nut shell and cassava binder. *Int J Educ Res* 7: 15–26.
23. Trubetskaya A, Leahy JL, Yazhenskikh E, et al. (2019) Characterization of woodstove briquettes from torrefied biomass and coal. *Energy* 171: 853–865.
24. Davies RM, Davies OA (2013) Physical and Combustion Characteristics of Briquettes Made from Water Hyacinth and Phytoplankton Scum as Binder. *J Combust* 2013: 549894.1–549894.7.
25. Hassan LG, Sani NA, Sokoto AM, et al. (2017) Comparative studies of burning rates and water boiling time of wood charcoal and briquettes produced from carbonized martynia annua woody shells. *Niger J Basic Appl Sci* 25: 21–27.

26. Oyelaran OA, Olorunfemi BJ, Sanusi OM, et al. (2018) Investigating the performance and combustion characteristics of composite Bio-coal Briquette. *J Mater Eng Struct* 5: 173–184.
27. Onukak IE, Mohammed-Dabo IA, Ameh AO, et al. (2017) Production and characterization of biomass briquettes from tannery solid waste. *Recycling* 2: 17.
28. Bruch C, Peters B, Nussbaumer T (2003) Modelling wood combustion under fixed bed conditions. *Fuel* 82: 729–738.
29. Patronellia S, Caposciutti G, Barontini F, et al. (2017) Experimental and numerical investigation of a small-scale fixed-bed biomass boiler. *Chem Eng Trans* 57: 187–192.
30. Barontini F, Galletti C, Di Mitri D, et al. (2018) Biomass combustion in a 140 kW fixed bed boiler: a joint experimental and modeling study. *Chem Eng Trans* 65: 55–60.
31. Meng X, Sun R, Ismail TM, et al. (2017) Parametric studies on corn combustion characteristics in a fixed bed: Primary air flow rate and different corn lengths. *Appl Therm Eng* 126: 702–716.
32. EN 12809: 2015 *Residential space heating appliances fired by wood pellets—Requirements and test methods*.
33. Coleman HW, Steele WG (2009) *Experimentation, Validation, and Uncertainty Analysis for Engineers*. 3rd Ed., New York, USA: John Wiley and Sons.
34. FprEN 14774-2:2009 *Solid biofuels—Determination of moisture content—Oven dry method—Part 2: Total moisture—Simplified method*.
35. Regueira LN, Aon JAR, Castieiras JP, et al. (2001) Determination of calorific values of forest waste biomass by static bomb calorimetry. *Thermochim Acta* 371: 23–31.
36. Nhuchhen DR, Abdul Salam P (2012) Estimation of higher heating value of biomass from proximate analysis: A new approach. *Fuel* 99: 55–63.
37. Field MA, Gill DW, Morgan BB, et al. (1967) *Combustion of Pulverised Coal*, Leatherhead, U.K.: The British Coal Utilisation Research Association (BCURA).
38. Smith IW (1982) The combustion rates of coal chars: A Review. *Symp (Int) on Combust* 19: 1045–1065.
39. Fennell PS, Kadchha S, Lee HY, et al. (2007) The measurement of the rate of burning of different coal chars in an electrically heated fluidised bed of sand. *Chem Eng Sci* 62: 608–618.
40. Turns S (2000) *An Introduction to Combustion: Concepts and Applications*, 2nd Ed., Singapore: McGraw Hill.
41. Szekely J, Evans JW, Sohn HY (1976) *Gas-Solid Reactions*, New York, USA: Academic Press.
42. Levenspiel O (1999) *Chemical Reaction Engineering*, 3rd Ed.; New York, USA: John Wiley and Sons.
43. Fogler HS (2006) *Elements of Chemical Reaction Engineering*, 4th Ed., Upper Saddle River, New Jersey, USA: Prentice Hall.
44. Lanfrey PY, Kuzeljevic ZV, Dudukovic MP (2010) Tortuosity model for fixed beds randomly packed with identical particles. *Chem Eng Sci* 65: 1891–1896.
45. Holman JP (1994) *Experimental Methods for Engineers*, 6th Ed., New York, USA: McGraw-Hill, Inc.
46. Wakao N, Funazkri T (1978) Effect of fluid dispersion coefficients on Particle-to-Fluid mass transfer coefficients in packed beds. Correlation of Sherwood Numbers. *Chem Eng Sci* 33: 1375–1384.
47. Borman GL, Ragland KW (1998) *Combustion Engineering*, New York, USA: McGraw-Hill International Editions.

48. Coelho P (2017) *Tabelas de Termodinâmica (In Portuguese)—Thermodynamic Tables*, 4th Ed., Lisbon, Portugal: Lidel, Edições Técnicas.